Ultrasonic triggering of giant magnetocaloric effect in MnAs thin films

J.-Y. Duquesne,[1] J.-Y. Prieur,[1] J. Agudo Canalejo,[1] V. H. Etgens,[1,2] M. Eddrief,[1] A. L. Ferreira,[1,3] and M. Marangolo[1]

[1]*Institut des NanoSciences de Paris, UPMC-CNRS UMR 7588, 4 place Jussieu, 75252 Paris Cedex 5, France*

[2]*Fédération Lavoisier Franklin, UVSQ, 45 avenue des Etats Unis, 78035 Versailles Cedex, France*

[3]*Departamento de Física, UFPR, Centro Politécnico, Caixa Postal 19091, 81531-990, Curitiba PR, Brazil*

(Received 31 January 2012; revised manuscript received 20 April 2012; published 12 July 2012)

Mechanical control of magnetic properties in magnetostrictive thin films offers the unexplored opportunity to employ surface wave acoustics in such a way that dynamic magnetic effects are triggered. Strain-induced modulation of the magnetic anisotropy can play a role in high-frequency varying effective magnetic fields, leading to ultrasonic tuning of electronic and magnetic properties of nanostructured materials, which eventually can be integrated into semiconductor technology. Here, we report on the opportunity to employ surface acoustic waves to trigger magnetocaloric effects in MnAs(100 nm)/GaAs(001) thin films. During the MnAs magnetostructural phase transition, in an interval range around room temperature (0°–60 °C), ultrasonic waves (170 MHz) are strongly attenuated by the phase coexistence (up to 150 dB/cm). We show that the giant magnetocaloric effect of MnAs is responsible for the observed phenomenon. By use of a simple anelastic model we describe the temperature and the external magnetic field dependence of such a huge ultrasound attenuation. Strain manipulation of the magnetocaloric effect could be a further interesting route for dynamic and static caloritronics and spintronics applications in semiconductor technology.

DOI: 10.1103/PhysRevB.86.035207 PACS number(s): 75.30.Sg, 43.35.Rw, 68.60.−p

I. INTRODUCTION

In the past few years, magnetism research in bulk materials and in nanostructures has cross-coupled magnetization with either local and noninductive fields or with thermally driven effects. The former experiments concern the use of electric fields to control local magnetization in multiferroic materials,[1] spin-polarized currents to generate radio-frequency (rf) coherent emission in nanopillars,[2] ultrafast pulsed lasers to create magnetic domains,[3] and self-organized templates to switch magnetization.[4] Latter experiments deal with a combination of electron spin and heat, such as spin-dependent Peltier[5] and Seebeck effects.[6] All these effects would allow new means to control local magnetic properties in spintronics devices, thereby avoiding cumbersome inductive means. Here, we report on a thermally driven effect induced by noninductive means in a magnetic thin film. We show that the well-known interaction of surface acoustic waves (SAWs) with magnetic excitations[7–9] is able to trigger MCE in MnAs. We argue that strain induces strong modifications of the inner magnetic field in this magnetoelastic material, inducing consequent MCE triggering.

II. MAGNETOCALORIC PROPERTIES OF MnAs

The magnetocaloric effect (MCE) is either an isothermal magnetic-entropy change or an adiabatic temperature change, obtained by applying an external magnetic field. MCE enables an efficient refrigeration process and would permit a low-cost and environmentally sustainable alternative to gas compression techniques.[10] Recently, our group has shown that MCE can be obtained in MnAs thin films and tailored by use of epitaxial strain engineering.[11] MnAs presents also a strong magnetoelastic coefficient that induces a magnetostructural transition around 40 °C in bulk MnAs, where the low-temperature hexagonal NiAs structure (α-MnAs) transforms into non-ferromagnetic orthorhombic β-MnAs by a first-order transition.[12] This magnetostructural phase transition is accompanied by one of the highest magnetocaloric effects, in the neighboring of room temperature:[13] 120 J Kg^{-1} K^{-1} for a magnetic field variation of 5 T. In MnAs/GaAs(001) thin films, magnetoelastic coupling is so intense that, over the temperature range 13 °C to 40 °C, MnAs/GaAs(001) displays an α/β-MnAs phase coexistence.[14,15] This phenomemon is due to epitaxial conditions.[16] The α/β phase coexistence induces a spreading of the magnetocaloric effect in a temperature range, centered around 35 °C.[11] The magnetic entropy change depends quite linearly on the applied magnetic field (see Fig. 3 in Ref. 11).

III. EXPERIMENTAL METHODS

Figure 1 displays the structure of the sample under study. MnAs epilayers were grown by MBE on GaAs(001) substrates. Epiready GaAs substrates were, first, deoxidized under As overpressure followed by GaAs buffer-layer growth in standard growth conditions. At the end, the surface was long annealed at 600 °C under As to optimize its quality, confirmed by the presence of a clear $(2 \times 4)\beta$ diagram as checked by reflection high-energy electron diffraction (RHEED). Next, we cooled down the sample and followed the procedure of Arai *et al.*[17] to obtain a stable and high-quality As-terminated c (4×4) surface. The MnAs growth was performed at 260 °C under As-rich conditions and a growth rate of about 3 nm/min. The epitaxial relationship was first verified *in situ* by use of RHEED and cross-checked *ex situ* by use of x-ray diffraction. MnAs displayed a single domain epitaxy from the beginning of the growth with [0001]MnAs//[1-10]GaAs. Finally, samples were protected by a few-nanometer Au capping layer. The sample was then introduced into a sputtering chamber, where a gold layer (∼200 nm) and a ZnO layer (∼2 μm) were deposited. The substrate temperature was around 200 °C. The gold layer was obtained by use of thermal evaporation. The

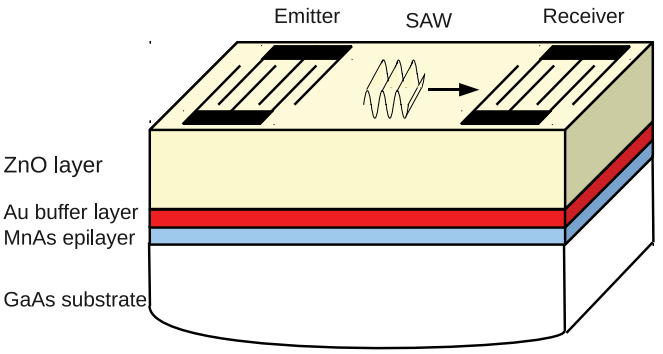

FIG. 1. (Color online) Structure of the sample (not to scale). MnAs epilayer, 100 nm; gold buffer, ≃300 nm; ZnO piezoelectric layer, ≃1 μm; excited wavelength, $\lambda = 15$ μm. The acoustic wave vector is parallel to the MnAs easy magnetic axis.

piezoelectric ZnO layer was obtained by rf sputtering from a Zn target in an $Ar + O_2$ plasma. The aim of the gold layer was to favor ZnO growth and to relax the constraints arising from the different dilatations of MnAs/GaAs and ZnO. The aim of the piezoelectric ZnO layer was to excite and detect surface acoustic waves, thanks to interdigital transducers (IDTs). IDTs are oriented in such a way where the acoustic wave vector is parallel to the easy magnetic axis of the MnAs α phase. ITDs are made by use of lift-off photolithography and thermal evaporation of gold (200 nm) onto a thin adhesion Cr layer. The period of the IDTs was 15 μm. The width of one IDTs tooth was 3.75 μm. The excited wavelength was 15 μm and the corresponding resonant acoustic frequency was 170 MHz. The distance between transducers was 2 mm. The aperture of the transducers was 2 mm. The emitter was excited at its resonant frequency (170 MHz) with a 500-ns rf burst. After propagation in the sample, the acoustic burst was detected by the receiver and the signal was processed using a phase detection scheme. Because of the velocity changes versus temperature or magnetic field, the resonant frequency of the transducers slightly shifts with temperature or field. However, we checked that the shift is small and has no affect on the measured attenuation variation, at fixed frequency. The typical cooling and warming rate is 1 °C/min.

IV. EXPERIMENTAL RESULTS

In a first set of experiments, the sample is demagnetized at 86 °C and zero-field cooled to 0 °C. The attenuation changes are then measured as a function of temperature, from 0 °C to 86 °C, and back to 0 °C. Thermal cycles are performed either in zero or nonzero applied field (0.2 T). Figure 2 displays the measured difference of ultrasound attenuation, $\Delta\Gamma$, with respect to a reference value at $T = 0$ °C. The most important experimental result of this paper is the huge attenuation peak (150 dB cm^{-1}) observed around 34 °C. The magnitude of this variation is surprising if one considers that the MnAs layer (100 nm) is roughly two orders of magnitude smaller that the penetration depth of the surface acoustic wave ($\sim\lambda = 15$ μm), so most of the acoustic energy is located in the substrate, not in the MnAs layer. The precise location of the peak slightly depends on whether the sample is warmed or cooled.

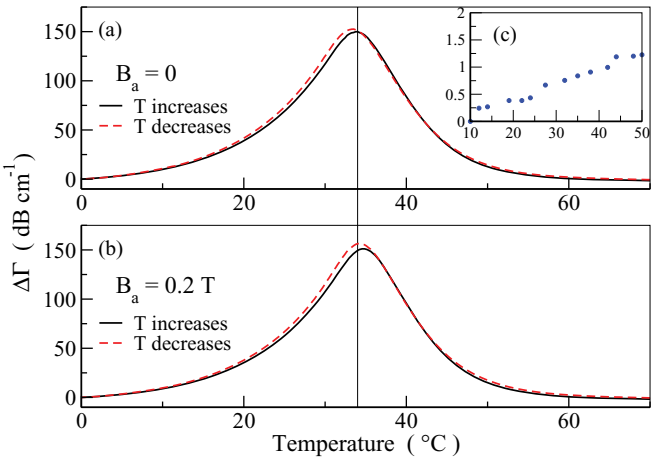

FIG. 2. (Color online) Variations of acoustic attenuation $\Delta\Gamma = \Gamma(T) - \Gamma(0\,°\mathrm{C})$ versus temperature T, at 170 MHz, for two different applied magnetic fields. (Inset) Attenuation changes $\Delta\Gamma = \Gamma(T) - \Gamma\,(10\,°\mathrm{C})$ in the MnAs free sample at 120 MHz.

Moreover, the attenuation curve is rigidly shifted to higher temperatures when an external field is applied,

$$\Delta T = \gamma_A B_a, \tag{1}$$

where $\gamma_A \simeq 4.6\,°\mathrm{C\,T^{-1}}$. For comparison, we measured the attenuation changes versus temperature in a similar hybrid structure but without MnAs. The Fig. 2 inset displays the result. No attenuation peak is observed and the attenuation variation is only around 1 dB cm^{-1} between 10 °C and 50 °C.

In a second set of experiments, we measured the isothermal attenuation versus the applied magnetic field. In that case, at every temperature, the sample is, first, magnetically cycled before the acoustic measurements are performed (cycle: 0 to 0.2 T to −0.2 T to 0 T). Figure 3 displays typical results. Hysteresis is observed at low fields but the overall behavior is a linear variation of attenuation versus applied field modulus. It is worthwhile noticing the striking correlation between the behaviors of attenuation $\Delta\Gamma$, versus either temperature T

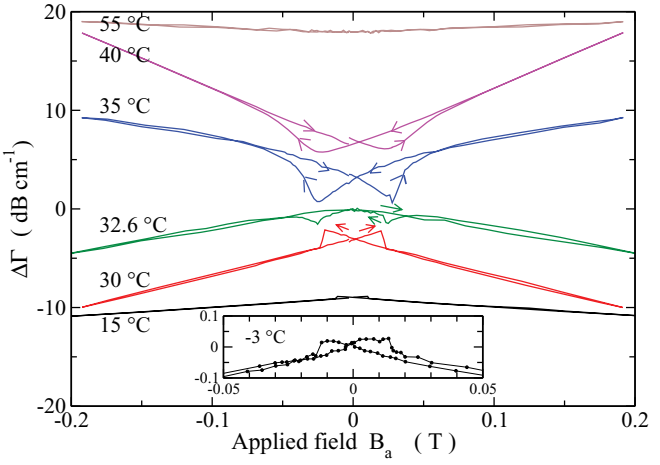

FIG. 3. (Color online) Isothermal attenuation variations $\Delta\Gamma = \Gamma(B_a) - \Gamma(B_a = 0)$, at 170 MHz, versus applied field. For clarity, curves are shifted along the attenuation axis. The arrows show the direction of the magnetic cycle. (Inset) $\Delta\Gamma$ at $T = -3$ °C.

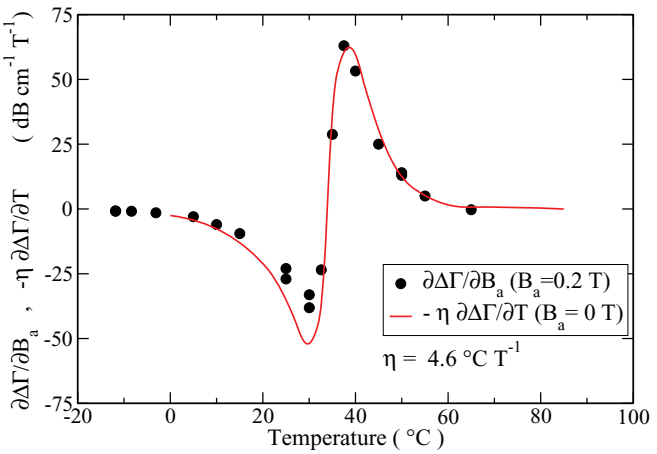

FIG. 4. (Color online) Temperature and field derivatives of the experimental acoustic attenuation.

or applied field B_a. Below 33 °C, $\Delta\Gamma$ increases if either T increases or B_a decreases. Above 33 °C, the reverse behavior is observed. The temperature and field derivatives are roughly proportional, as shown in Fig. 4:

$$\frac{\partial \Delta\Gamma}{\partial B_a} \simeq -\eta \frac{\partial \Delta\Gamma}{\partial T}. \tag{2}$$

We find $\eta = 4.6\,^{\circ}\mathrm{C\,T^{-1}} = \gamma_A$. It can be shown that this a direct consequence of Eq. (1).

V. DISCUSSION

We argue here that the behavior of the acoustic wave is due to a thermoelastic effect, enhanced by the magnetoelastic and magnetocaloric properties of MnAs. These two points will now be successively discussed.

Let us, first, consider the attenuation of sound due to a relaxation process. Quite generally, it can be inferred from a quasistatic stress-relaxation experiment where a strain ϵ is suddenly applied and held constant.[18] The stress σ instantaneously changes from 0 to $C_U\epsilon$ and then relaxes to $C_R\epsilon$ with a characteristic time τ. C_U and C_R are the instantaneous and relaxed elastic modulus, respectively, and it is useful to define $\Delta C = C_U - C_R$. The sound amplitude decay α, defined by the displacement change $u(x) = u(0)\exp(-\alpha x)$ along the x spatial coordinate, can be inferred,[18]

$$\alpha = \frac{\Delta C}{2\rho v^3} \frac{\omega^2\tau}{1+\omega^2\tau^2} \tag{3}$$

$\omega/2\pi$, v, and ρ are the acoustic frequency, the wave velocity and mass density, respectively. The acoustic attenuation expressed in dB per unit length is $\Gamma = (20\alpha/\ln 10) \simeq 8.7\alpha$. The expression of ΔC depends on the relaxation mechanism. Thermoelastic relaxation is a well-known process for sound absorption due to heat transfer between regions exhibiting different strains. In that case, the entropy density is the internal variable which relax on application of strain.[18] Its equilibrium value s depends on the state of strain and the equilibrium time is τ. It can be shown that

$$\Delta C = \frac{-1}{\alpha_s}\left(\frac{\partial s}{\partial \epsilon}\right)_T, \tag{4}$$

where α_s is the linear thermal expansion coefficient at constant entropy. The thermal expansion factor α_s is weakly temperature dependent because the MnAs average lattice parameter follows the thermal lattice expansion of the GaAs substrate.[19] We assume that τ arises from heat transfer from MnAs to the GaAs substrate and Au/ZnO layers and to the heat diffusion inside those media. It is estimated to be around 10^{-11} s and is also weakly temperature dependent.[20] Consequently, we get $\omega\tau \ll 1$ and

$$\alpha = \frac{-1}{2\rho v^3 \alpha_s}\left(\frac{\partial s}{\partial \epsilon}\right)_T \omega^2\tau. \tag{5}$$

Therefore, $(\partial s/\partial\epsilon)_T$ is the leading parameter which governs the thermoelastic attenuation versus temperature or applied field. An expression which will be useful later comes from the Maxwell thermodynamical relation,

$$\left(\frac{\partial s}{\partial \epsilon}\right)_T = -\left(\frac{\partial \sigma}{\partial T}\right)_\epsilon. \tag{6}$$

Let us now consider the magnetic properties. In a magnetostrictive material, acoustic strain field induces a modification of the internal magnetic field. Here, we propose that this field modulation triggers a dynamic magnetocaloric effect in MnAs, responsible for large entropy and heat production. This enhances thermoelastic attenuation. The following experimental and theoretical observations suggest a magnetic excitations scenario.

(i) The open hysteresis of Fig. 3 attests that we deal with a magnetic phenomenon determined by the MnAs thin film. It is worthwhile emphasizing that the measured coercitive fields are in good agreement with the values derived from independent Kerr measurements (not shown here). Moreover, no large attenuation changes are observed in a similar sample, without the MnAs layer (see the Fig. 2 inset).

(ii) We underline the strong analogies between the attenuation and the field-induced magnetic entropy changes $\Delta s_m = s_m(B,T) - s_m(0,T)$ which has been measured in MnAs thin films by Mosca *et al.*[11] Both exhibit an extrema value and are symmetric with respect to ≃33 °C. Both exhibit high values at high temperatures (≃45 °C) and are magnetic field dependent (Fig. 3), despite the low α-MnAs fraction value. No saturation trend is observed at higher fields.

(iii) It has been shown that Δs_m is approximately equal to the total entropy change at the MnAs phase transition, indicating the important role of the magnetocaloric effect.[21]

We now show, qualitatively and quantitatively, that the magnetoelastic and magnetocaloric properties of MnAs thin films can explain the behavior of surface acoustic waves that we have observed.

Obviously, in Eqs. (4)–(6), s is the total entropy density. It includes the structural entropy of the substrate as well as the averaged value of the structural and magnetic entropy s_α and s_β of the pure α and β phases. To get ΔC from the strain dependence of each term would be a heroic task. We choose to adopt a pragmatic procedure by applying the Maxwell relation (6) to the temperature-dependent stress measurements published by Das *et al.*[22] These authors measured the temperature dependence of the total stress along the a axis of MnAs thin films. Dashed line in Fig. 5 reports the temperature derivative curve that we extracted from their published data,

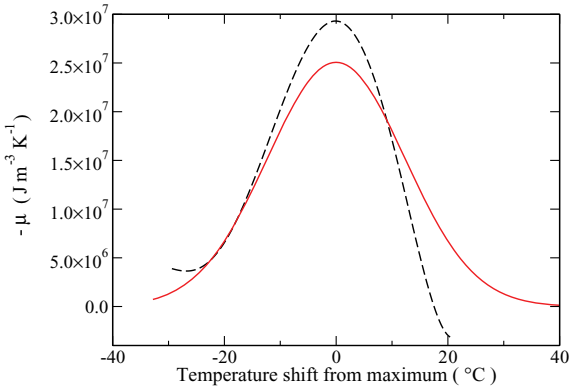

FIG. 5. (Color online) (Dashed line) $\mu = (\partial s/\partial\epsilon)_{\epsilon=0}$ derived from Das *et al.*[22] (Continuous line) ($\mu = \partial\Delta s_m/\partial\epsilon)_{\epsilon=0}$ derived from Mosca *et al.*[11] Temperatures of the maxima differ in 3 °C due to different samples or experimental methods.

i.e., $(\partial s/\partial\epsilon)_T$. The reader has to take into account that these measurements were done on MnAs thin films presenting a slighty lower transition temperature range as compared to our sample.

To get a more direct insight into the variations of entropy induced by strain, we consider magnetocaloric measurements. In Ref. 11, the magnetic entropy change as a function of temperature and magnetic field was extracted from magnetization versus temperature measurements. The magnetic entropy change follows the empirical expression between 15 °C and 55 °C:[23]

$$\Delta s_m(B_a,T) = -cB_a \exp -\left(\frac{\Delta T - \gamma B_a}{d}\right)^2, \qquad (7)$$

where B_a is the applied magnetic field (magnetic flux density), parallel to the easy magnetic axis of MnAs; T is the temperature; and $\Delta T = (T - T_0)$, where T_0 is a reference temperature. The fitting parameters are $c \simeq 2.82 \times 10^4$ J m^{-3} K^{-1} T^{-1}, $T_0 \simeq 33$ °C, $d \simeq 17.4$ °C, $\gamma \simeq 1.8$ °C T^{-1}. (We converted the entropy data units from J kg^{-1} K^{-1} to J m^{-3} K^{-1}, using MnAs mass density 6300 kg m^{-3}.) We notice the entropy curve shifts with B_a. Below in the text, we will show that this Δs_m shift leads to the attenuation peak shift that we have observed (4.6 °C T^{-1}). It also recalls the α-fraction shift versus magnetic field observed by Iikawa *et al.*,[24] with the same order of magnitude (5 °C T^{-1}). The same group reported a similar shift equal to $\delta\epsilon$, where ϵ is the strain applied along the MnAs easy axis and δ is temperature independent between 30 °C and 40 °C (see Fig. 3 in Ref. 25) with $\delta \simeq 1600$ °C. Thus, we postulate that an applied strain ϵ is equivalent to an effective field $B_\epsilon = (\delta/\gamma)\epsilon$, where $\delta/\gamma \simeq 900$ T. Consequently, the strain dependance of Δs_m is merely obtained by replacing B_a with $B_a + (\delta/\gamma)\epsilon$ in Eq. (7):

$$\Delta s_m(B_a,T,\epsilon) = -c\left(B_a + \frac{\delta}{\gamma}\epsilon\right) \exp -\left(\frac{\Delta T - \gamma B_a - \delta\epsilon}{d}\right)^2. \qquad (8)$$

Using this relation, $(\partial\Delta s_m/\partial\epsilon)_{T,\epsilon=0}$ can be readily derived,

$$\left(\frac{\partial\Delta s_m}{\partial\epsilon}\right)_{T,\epsilon=0} = -\frac{\delta}{\gamma}c\left[1 + \frac{2\gamma}{d^2}B_a\,(\Delta T - \gamma B_a)\right] \times \exp -\left(\frac{\Delta T - \gamma B_a}{d}\right)^2. \qquad (9)$$

Figure 5 displays $(\partial\Delta s_m/\partial\epsilon)_{T,\epsilon=0}$ derived from (9) at zero applied field ($B_a = 0$). Direct comparison can be done with $(\partial s/\partial\epsilon)_{T,\epsilon=0}$ derived previously from Das *et al.* results.[22] We notice that the magnitude and width of both curves are very close, despite the different samples and experimental apparatus. This demonstrates that the main contribution to strain-induced entropy change comes from the magnetic entropy term. Consequently, ultrasonic attenuation α [Eq. (5)] is such that

$$\alpha \propto \left(\frac{\partial s}{\partial\epsilon}\right)_T \simeq \left(\frac{\partial\Delta s_m}{\partial\epsilon}\right)_T. \qquad (10)$$

This result is consistent with the aforementioned theoretical calculations by Zou *et al.*[21] Strain modifies the equilibrium state of MnAs, inducing MCE, heat flow, and anelastic ultrasonic attenuation.

A number of features can be derived theoretically from Eqs. (5), (9), and (10) which corroborate the following scenario.

(i) Ultrasonic attenuation order of magnitude

By using Eq. (5), we can roughly estimate the magnitude of the attenuation peak. Indeed, this equation is valid for plane waves. In our case, the magnetocaloric energy transferred through the MnAs/GaAs or MnAs/Au/ZnO interfaces is diluted in the penetration depth. Thus, we have to normalize Eq. (5) by a geometrical factor $e/\lambda = 0.1\ \mu$m/15 μm where e is the MnAs film thickness. By using GaAs parameters,[26] we estimate $\Delta\Gamma = 8.7\alpha \simeq 150$ dB cm^{-1} at the maximum, in good agreement with the experimental result. This strongly supports that MCE in such a thin MnAs film can induce a huge effect on SAWs, even if the perfect agreement has to be considered as fortuitous because of the roughness of our approach.

(ii) Ultrasonic attenuation field dependence

Using Eq. (9) and keeping the leading terms, we derive

$$\frac{\partial\alpha}{\partial B_a} \propto \frac{\partial}{\partial B_a}\left(\frac{\partial\Delta s_m}{\partial\epsilon}\right)_{\epsilon=0} = -\frac{4c\delta}{d^2}\left(\Delta T - \frac{3}{2}\gamma B_a + g(\Delta T, B_a)\right) \times \exp -\left(\frac{\Delta T - \gamma B_a}{d}\right)^2, \qquad (11)$$

where $g(\Delta T, B_a) = \gamma B_a(\Delta T - \gamma B_a)^2/d^2$. Equation (11) shows that, in our experimental field range ($B_a < 0.2$ T) and for ΔT larger than $\gamma B_a = 0.36$ °C, $\partial\alpha/\partial B_a$ is independent of the field: Acoustic attenuation α is a linear function of the applied field, in good agreement with experiments (Fig. 3). From Eqs. (9) and (11), we can safely do the following approximation: $(\partial\alpha/\partial B_a)/\alpha \simeq (4\gamma/d^2)\Delta T$. Theoretical and experimental values are in the same order of magnitude, which is quite satisfactory, due to the roughness of our model: 0.2 and 0.6 dB cm^{-1} T^{-1}, respectively.

(iii) Peak temperature dependence

Using Eq. (9) and keeping the leading terms, we derive

$$\frac{\partial\alpha}{\partial T} \propto \frac{\partial}{\partial T}\left(\frac{\partial \Delta s_m}{\partial \epsilon}\right)_{\epsilon=0} = \frac{2c\delta}{\gamma d^2}\left[\Delta T - 2\gamma B_a + 2g(\Delta T, B_a)\right] \times \exp - \left(\frac{\Delta T - \gamma B_a}{d}\right)^2. \quad (12)$$

Using Eq. (12), it is straightforward to show that a good approximation for the maximum location is given by $(\Delta T - 2\gamma B_a) = 0$. Our calculation then predicts a $2\gamma = 3.6\ \mathrm{K}^{-1}\ \mathrm{T}^{-1}$ attenuation shift with applied field. The experimental shift is $\gamma_A = 4.6\ \mathrm{K}^{-1}\ \mathrm{T}^{-1}$. Again, due to the roughness of our model, the agreement is quite good.

Finally, it is worthwhile reporting that our model is able to predict Eq. (2) and, therefore, to establish a connection between the field-induced temperature shifts of both ultrasonic attenuation and entropy changes. Indeed, using Eqs. (5), (11), and (12), we get (in our experimental field range and for ΔT larger than a few degrees)

$$\frac{\partial\alpha}{\partial B_a} \simeq -2\gamma \frac{\partial\alpha}{\partial T}. \quad (13)$$

A comparison with Eq. (2) gives $\eta = \gamma_A = 2\gamma$.

VI. CONCLUSION

In conclusion, ultrasound surface waves are a hitherto unexplored means to modulate thermal properties in magnetocaloric thin films, at high frequency, without using cumbersome and energy-consuming inductive means. We have shown that the huge ultrasound attenuation observed on thin MnAs films epitaxied on GaAs(001) can be ascribed to the strain-induced triggering of the giant magnetocaloric effect of MnAs. In short, we have shown that acoustic stresses induce local thermodynamical changes in the MnAs and GaAs media. This changes have a magnetocaloric origin in MnAs despite the very low quantity of magnetic material in the heterostructure. To restore equilibrium, a heat flow sets up. Heat transfer is very rapid. We anticipate that piezoelectric technology opens up a new way to control magnetocaloric and spin caloric phenomena, even at high frequencies, in ferromagnet/piezoelectric/semiconductor hybrid systems. Applications to nonvolatile magnetic storage functionality, fast signal processing, thermal sensors, magnetic sensors, and microwave filtering can be envisaged.

ACKNOWLEDGMENTS

The authors thank M. Sacchi, F. Vidal, and D. H. Mosca for fruitful discussions. A. L. Ferreira acknowledges support from CAPES-COFECUB. We warmly thank R. Gohier for technical assistance and M. Brossard and S. Vercauteren for their involvements during their master internships.

[1] Y.-H. Chu, L. W. Martin, M. B. Holcomb, M. Gajek, S.-J. Han, Q. He, N. Balke, C.-H. Yang, D. Lee, W. Hu, Q. Zhan, P.-L. Yang, A. Fraile-Rodriguez, A. Scholl, S. X. Wang, and R. Ramesh, Nat. Mater. **7**, 478 (2008).

[2] L. Berger, Phys. Rev. B **54**, 9353 (1996).

[3] J. A. de Jong, I. Razdolski, A. M. Kalashnikova, R. V. Pisarev, A. M. Balbashov, A. Kirilyuk, T. Rasing, and A. V. Kimel, Phys. Rev. Lett. **108**, 157601 (2012).

[4] M. Sacchi, M. Marangolo, C. Spezzani, R. Breitwieser, H. Popescu, R. Dealaunay, B. Rache Salles, M. Eddrief, and V. H. Etgens, Phys. Rev. B **81**, 220401 (2010).

[5] L. Gravier, S. Serrano-Guisan, F. Reuse, and J. P. Ansermet, Phys. Rev. B **73**, 052410 (2006).

[6] K. Uchida, T. Ota, K. Harii, S. Takahashi, S. Maekawa, Y. Fujikawa, and E. Saitoh, Sol. State Comm. **150**, 524 (2010).

[7] S. Davis, A. Baruth, and S. Adenwalla, Appl. Phys. Lett. **97**, 232507 (2010)

[8] M. Weiler, L. Dreher, C. Heeg, H. Huebl, R. Gross, M. S. Brandt, and S. T. B. Goennenwein, Phys. Rev. Lett. **106**, 117601 (2011).

[9] R. Huber, P. Klemm, S. Neusser, B. Botters, A. Wittmann, M. Weiler, S. T. B. Goennenwein, C. Heyn, M. Schneider, P. Boeni, and D. Grundler, Sol. State Comm. **150**, 492 (2010).

[10] K. A. Gschneidner Jr., V. K. Pecharsky, and A. Tsokol, Rep. Prog. Phys. **68**, 1479 (2005).

[11] D. H. Mosca, F. Vidal, and V. H. Etgens, Phys. Rev. Lett. **101**, 125503 (2008).

[12] C. P. Bean and D. S. Rodbell, Phys. Rev. **126**, 104 (1962).

[13] P. J. von Ranke, S. Gama, A. A. Coelho, A. de Campos, A. M. G. Carvalho, F. C. G. Gandra, and N. A. de Oliveira, Phys. Rev. B **73**, 014415 (2006).

[14] V. M. Kaganer, B. Jenichen, F. Schippan, W. Braun, L. Däweritz, and K. H. Ploog, Phys. Rev. B **66**, 045305 (2002).

[15] R. Breitwieser, F. Vidal, I. L. Graff, M. Marangolo, M. Eddrief, J.-C. Boulliard, and V. H. Etgens, Phys. Rev. B **80**, 045403 (2009).

[16] L. Daeweritz, Rep. Prog. Phys. **69**, 2581 (2006).

[17] T. Arai, M. Suzuki, Y. Ueno, J. Okabayashi, and J. Yoshino, Physica E **40**, 332 (2007).

[18] A. S. Nowick and B. S. Berry, *Anelastic Relaxation in Crystalline Solids* (Academic Press, New York/London, 1972).

[19] V. Garcia, Y. Sidis, M. Marangolo, F. Vidal, M. Eddrief, P. Bourges, F. Maccherozzi, F. Ott, G. Panaccione, and V. H. Etgens, Phys. Rev. Lett. **99**, 117205 (2007).

[20] A given amount of thermal energy is driven in the thin film. We solve then the heat diffusion equation to monitor the heat transfert rate τ in the substrate. It turns out that $\tau = e^2\rho_f^2 C_f^2 D_s/K_s^2 \simeq 10^{-11}$ s, where e, ρ_f, C_f are the thickness, mass density, and specific heat of MnAs, D_s, K_s are the thermal diffusivity and conductivity of GaAs.

[21] J. D. Zou, H. Wada, B. G. Shen, J. R. Sun, and W. Li, Eur. Phys. Lett. **81**, 47002 (2008).

[22] A. K. Das, C. Pampuch, A. Ney, T. Hesjedal, L. Däweritz, R. Koch, and K. H. Ploog, Phys. Rev. Lett. **91**, 087203 (2003).

[23] The gaussian fit is a rough approximation of Δs_m for $B_a < 2$ T, but it catches the salient physics: maxima versus temperature, width

of the curves, maximum amplitude versus field, and maximum temperature shift versus field.

[24]F. Iikawa, M. Knobel, P. V. Santos, C. Adriano, O. D. D. Couto, M. J. S. P. Brasil, C. Giles, R. Magalhães-Paniago, and L. Daweritz, Phys. Rev. B **71**, 045319 (2005).

[25]F. Iikawa, M. J. S. P. Brasil, C. Adriano, O. D. D. Couto, C. Giles, P. V. Santos, L. Däweritz, I. Rungger, and S. Sanvito, Phys. Rev. Lett. **95**, 077203 (2005).

[26]GaAs parameters: $\alpha_s = 6 \times 10^{-6}$ K^{-1}, mass density $=$ 5300 kg m^{-3}, SAW velocity $=$ 2600 m s^{-1}.